L-shell ionization in near-central collisions of MeV protons with low-Z atoms

M. Kavčič, Ž. Šmit, and M. Budnar
J. Stefan Institute, P.O. Box 3000, SI-1001 Ljubljana, Slovenia

Z. Halabuka
Institute of Theoretical Physics, University of Basel, CH-4056 Basel, Switzerland
(Received 16 June 1997)

High-resolution $K\alpha$ x-ray spectra of Ca, Cr, and Fe induced by (0.7–1.5)-MeV protons and of Ti induced by (0.7–4)-MeV protons were measured by a flat crystal spectrometer. From the relative yields of the KL^1 satellites, which are the result of multiple inner-shell ionization, the average L-shell ionization probabilities in near-central collisions were determined. The effects of the rearrangement of the inner-shell holes prior to the K x-ray emission and the changes of the fluorescence yields due to the multiple ionization were taken into account in the evaluation of the ionization probabilities. The direct Coulomb ionization probabilities in the near-central collisions were determined from the relative yields of the KL^1 satellites after subtracting the shake contribution. The values obtained were compared with semiclassical approximation calculations exploiting relativistic hydrogenic and Hartree-Fock wave functions. The importance of a realistic atomic description using Hartree-Fock wave functions was demonstrated. [S1050-2947(97)01512-6]

PACS number(s): 32.80.Hd, 32.30.Rj, 34.50.Fa

I. INTRODUCTION

The inner-shell ionization induced by proton collisions with light atoms is mainly a result of the direct Coulomb interaction between the inner-shell electron and the moving projectile. This interaction perturbs the atomic potential and may result in the ejection of inner-shell electrons. In the case of high-energy projectiles, several inner-shell vacancies can be created in the collision. In the subsequent radiative transitions of such multiply ionized states, these additional spectator vacancies change the electron binding energies. The resulting x-ray lines are characterized as satellites since they are shifted towards higher energies compared to the energies of the diagram lines in singly ionized atoms.

For a given atom, the magnitude of the energy shift depends on the configuration of the spectator vacancies in the inner shells. When the additional vacancies are created in the shell involved in the transition, the energy shift is usually larger than the natural linewidth. Using a high-resolution crystal diffraction spectrometer, the satellite lines on the high-energy side of the diagram line, which correspond to the transitions in multiply ionized atoms, can be resolved from the diagram lines. The vacancies created in such an ion-atom collision are populated statistically, so the K x-ray spectra generally show a complex satellite structure, depending on the properties of the projectile and the target atom.

The KL^n satellites in the K x-ray spectra are related to the electron transitions in the atom with a singly ionized K shell and a multiply ionized L shell. The relative yield distribution of the KL^n satellite lines is directly related to the L-shell ionization probabilities and may yield information about the ionization mechanism as well as about the correlation effects in the atom. In the case of charged-particle impact, the L-shell ionization probability varies very slowly across the impact-parameter region where the K-shell ionization may occur. We can then treat the collisions resulting in the KL^n state as nearly central (i.e., with zero impact parameter) with respect to the L-shell impact-parameter scale. In deducing the original L-shell vacancy distribution created in the collision, the changes of the fluorescence yields and especially the rearrangement of the L-shell vacancies prior to the K x-ray emission have to be taken into account. From the original vacancy yield ratios deduced from the relative yields of the KL^n satellite lines, the L-shell ionization probability in near-central collisions can be evaluated. This provides a much better test of theoretical descriptions than measurements of the total cross sections since the possible differences between theory and experiment can be smeared out in the integration over the whole impact-parameter range. Satellite measurements are also advantageous compared to those of the total cross section since they do not require a very accurate knowledge of the fluorescence yields that may have large uncertainties, mainly due to the Auger level width uncertainties. These uncertainties influence the evaluation of the ionization probabilities only through the calculation of the rearrangement factors.

Studies of charged-particle-induced inner-shell ionization through x-ray satellites were initiated about 30 years ago when MeV energy accelerators were increasingly used for atomic physics studies. Many papers, e.g., [1–6], were directed towards an understanding of the multiple ionization of low-Z atoms by light ions. Many recent studies [7–10] stretched the research interests towards medium-Z targets and applied heavier ions as projectiles.

The basic goal of this work is to determine the L-shell ionization probability arising from direct Coulomb ionization in proton collisions with low-Z elements, being aware that important processes such as the rearrangement of vacancies prior to photon emission are taking place during the ionization-decay process. Our interest was stimulated by significant discrepancies between the old experimental data and recent theoretical predictions. The data obtained in the

present experiment were compared with semiclassical approximation (SCA) calculations using hydrogenic [11–14] and Hartree-Fock (HF) wave functions [15]. In the comparison of calculated and measured data, we showed the importance of using realistic HF wave functions for the atomic description. The ionization probability was studied as a function of the reduced projectile velocity, which was defined as the ratio of the projectile and the L-shell electron velocity. The differences between theory and experiment were clearly velocity dependent.

In the present paper we describe first the experimental setup in Sec. II followed by a description of the spectrum analysis in Sec. III. The method of deducing ionization probabilities from the measured relative yields of the KL^1 satellite line is presented in Sec. IV. We conclude with the results and a comparison with the SCA calculations in Sec. V. The justification of choosing an appropriate set of wave functions is described.

II. EXPERIMENT

The $K\alpha$ x-ray spectra of Ca, Ti, Cr, and Fe ionized with (0.7–1.5)-MeV protons were measured at the J. Stefan Institute, Ljubljana, using a high-resolution crystal spectrometer. Protons were accelerated by a 2-MV Van de Graaff accelerator. The obtained results stimulated us to perform further measurements at the Ruder Bošković Institute in Zagreb. With their 6-MV Tandem accelerator, Ti $K\alpha$ spectra with proton energies up to 4 MeV were measured.

The high-resolution x-ray spectrometer, already used for several other atomic physics studies [16–18], is described in detail elsewhere [16]. It consists of a vacuum irradiation chamber in which the measured samples are inserted, a vacuum chamber with the diffraction crystal that is evacuated separately in order to reduce the absorption of x rays, and the position-sensitive detector (PSD) for the detection of diffracted x rays. The three units were separated by kapton windows and air gaps with total thicknesses of 75 μm and 12 mm, respectively.

The protons impinged the thick metal target perpendicularly. The targets, made of pure Ca, Ti, Cr, and Fe were polished before they were inserted into the irradiation chamber. The Ca surface oxidized during the measurements (the estimated thickness of oxide was 0.1 μm) and all the targets became covered with a thin layer of carbon due to the nonideal vacuum conditions in the accelerator vacuum system ($\sim 10^{-6}$ mbar). The outcoming x rays were diffracted in first order on a flat LiF crystal. The dimensions of the crystal were 75×30 mm^2 and its thickness was 4 mm. The $\langle 200\rangle$ reflecting planes were used for Ca and Ti and the $\langle 220\rangle$ reflecting planes for Cr and Fe. The reflected x rays were detected by the position-sensitive detector. The dimensions of the PSD entrance window made of the aluminized Mylar foil (6 μm of Mylar foil and 50 nm Al) were 130×10 mm^2. The PSD was of proportional type using an $Ar(90\%)+CH_4(10\%)$ mixture as the working gas. The delay line arrangement, tightly mounted on the cathode circuit, which consisted of 50 cathode strips, was employed for an accurate position determination of the absorbed x ray. The start signal was provided from the anode wire, coupled to a charge-sensitive amplifier. The stop signal was provided similarly from the cathode strips through the delay line. The time difference between the two signals is proportional to the lateral position of the detected x ray. Using constant fraction discriminators, a good time resolution was achieved, resulting in a lateral resolution of 0.4 mm.

The intrinsic resolution of the spectrometer, determined mainly by the spatial resolution of the position-sensitive detector, was 2.2–3.3 eV. The distance between the target and the PSD was 866 mm, which resulted in very good angular resolution. The lateral dimensions of the PSD were 12 cm, which allowed a (300–400)-eV-wide energy interval to be measured within a single run. The experimental energy resolution depended mainly on the dimensions of the beam spot on the target, which was $(0.5–0.7)\times 10$ mm^2. This size implied an energy resolution of 3.5–6.5 eV, which was sufficient for clearly resolving the KL^1 satellites from the diagram lines.

III. DATA ANALYSIS

The measured $K\alpha$ spectra exhibit additional lines on the high-energy tail of the diagram line (Fig. 1). These lines are classified as the KL^n satellites of the $K\alpha$ line and correspond to the $K\rightarrow L_{\mathrm{II,III}}$ transitions in a multiply ionized atom with n additional vacancies in the L shell. In the case of proton-induced ionization, the L-shell ionization probabilities are rather small ($\sim 1\%$) and imply the excitation of the KL^1 doubly ionized states only; however, in the case of Ca a small contribution from the KL^2 state was also observed. A typical spectrum consisted of the $K\alpha_{1,2}$ diagram lines and the KL^1 satellite line on the high-energy tail of the diagram line. The measured spectra of Ca, Ti, Cr, and Fe are represented in Fig. 1.

In the independent-particle framework, the probability that a proton with an impact parameter b produces m vacancies in the K shell and n vacancies in the L shell can be expressed by the binomial distribution [19]

$$P_{mK,nL}=\binom{2}{m}\binom{8}{n}[p_K(b)]^m[1-p_k(b)]^{2-m}\times[p_L(b)]^n[1-p_L(b)]^{8-n}, \tag{1}$$

where p_K is the K-shell ionization probability per electron and p_L is the mean ionization probability per electron for the three L subshells. To obtain the cross section, the probability is integrated over the impact parameter

$$\sigma_{K^m,L^n}=2\pi\int_0^\infty\binom{2}{m}\binom{8}{n}[p_K(b)]^m[1-p_K(b)]^{2-m}\times[p_L(b)]^n[1-p_L(b)]^{8-n}b\,db. \tag{2}$$

Since the L-shell ionization probability is nearly constant over the impact parameter region where K-shell ionization may occur, we obtain

$$\sigma_{K^m,L^n}=2\pi\binom{8}{n}[p_L(0)]^n[1-p_L(0)]^{8-n}\int_0^\infty\binom{2}{m}\times[p_K(b)]^m[1-p_K(b)]^{2-m}b\,db. \tag{3}$$

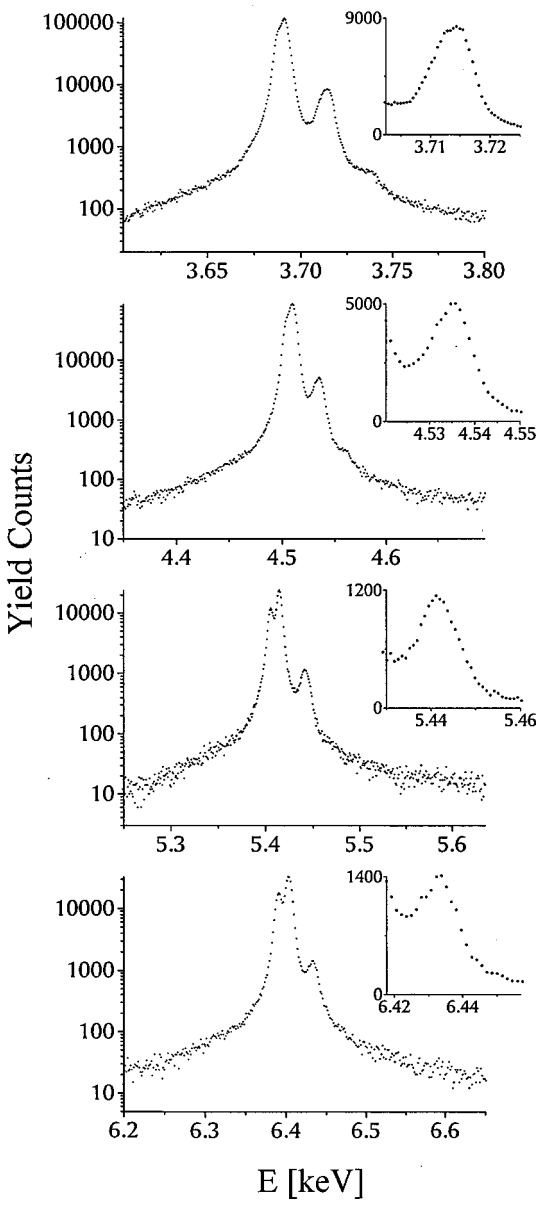

FIG. 1. High-resolution $K\alpha$ spectrum of Ca, Ti, Cr, and Fe, induced by 1.5-MeV protons, with an enlarged view of the KL^1 satellite line (upper corner of the inset). Some asymmetry on the low-energy tail of the diagram line is due to the KLM radiative Auger effect.

Considering that the primary vacancy yield I_{KL^n} is proportional to the ionization cross section σ_{KL^n}, one obtains

$$\frac{I_{KL^n}}{I_{KL^0}}=\frac{\sigma_{KL^n}}{\sigma_{KL^0}}=\frac{\binom{8}{n}[p_L(0)]^n}{[1-p_L(0)]^n}. \tag{4}$$

It is evident that the KL^n satellite yield relative to the $K\alpha$ diagram line gives us the L-shell ionization probability for the near-central collisions (zero impact parameter) within the independent-particle framework.

The $K\alpha$ x-ray spectra of multiply ionized atoms are very complex. The different configurations of the L-shell vacancy among the three L subshells and the different angular momentum couplings of the inner-shell vacancies are responsible for energy splitting of both the initial and final states. The transition may therefore occur between many different states, resulting in a rich spectrum structure. The shape of the lines can also be affected by M-shell ionization, although in our case this contribution was not significant. For a proper spectrum analysis, a theoretical knowledge of the $K\alpha L^n$ structure is needed [10]. In the case of low-Z element ionization, this fine structure is usually almost completely smeared out due to the energy resolution of the spectrometer, which is typically a few eV. This fine structure cannot be completely resolved even by better instrumental resolution since we cannot remove the effects of natural linewidths. As we focused our interest on the yield of the KL^1 satellite line relative to the $K\alpha$ diagram line, the spectra were separated into three components. The $K\alpha_1$ and $K\alpha_2$ lines were analyzed using two Voigt functions. The Voigt function is the convolution of the Lorentzian and Gaussian distribution, corresponding to the natural line shape and the instrumental response, respectively. The Lorentzian widths of the $K\alpha_1$ and $K\alpha_2$ lines were assumed to be equal, but let free through the fit. If the tabulated values of the Lorentzian widths were included in the fit, the response function of the spectrometer had to be known very precisely. The response of the spectrometer is usually well described by a Gaussian distribution, but it is almost impossible to avoid some deviations in the tails. This is the reason that the Lorentzian widths obtained from the fit are slightly larger than the natural line widths that can be found in tables. The KL^1 satellite was described by a single Voigt function, but the widths of both the Lorentzian and Gaussian component were left free. In order to estimate the reliability of our fitting model, we compared the yields obtained from the fits using either single or multiple Voigt functions, which in the latter case described the strongest contributions to the KL^1 satellite line as given in the literature [20]. The two procedures gave total KL^1 line yields, which differed by less than 3%, which implied that the fit using a single Voigt function provides reliable results.

From the fitting procedure we evaluated the KL^1 satellite yields with respect to the $K\alpha$ diagram lines. Figure 2 shows a high-resolution $K\alpha$ x-ray spectrum of Fe, bombarded with 1-MeV protons, fitted with the model described above. The EWA program package for spectrum analysis [21] was used for spectrum fitting.

After the fitting procedure, several experimental corrections of the relative satellite yields were applied. Because of the targets used were thick, we had to account for proton stopping and x-ray absorption in the target. The relative satellite yields deduced from thick targets were converted into their respective thin target values by the use of correction factors. They were calculated following the Merzbacher-Lewis formula [22]. The derivative dE/dx as required by [22] was calculated from the fit to the measured data. For Ti, where the yield varies smoothly with proton energy, the correction factor differed from unity by 3%, but for the Fe, where the energy dependence of the yield is more pronounced, this difference was about 10%. The stopping powers of Ziegler and Manoyan [23] were used. The x-ray attenuation coefficients were obtained from the tables of Thinh and Leroux [24].

The relative satellite yields were also corrected for x-ray absorption in the three 25-μm Kapton foils and a 12-mm air gap between the target and detector, for the crystal reflectiv-

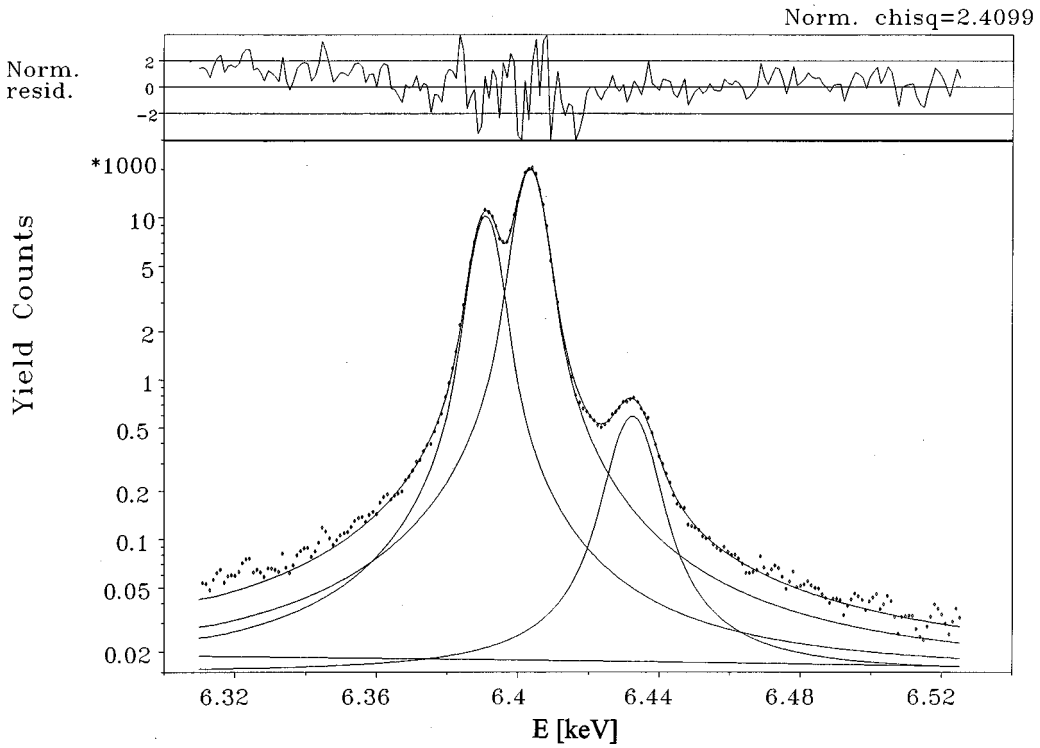

FIG. 2. Fe $K\alpha$ spectrum induced by 1.0-MeV protons, decomposed by the fitting method as explained in Sec. III. The $K\alpha_1$ and $K\alpha_2$ lines are fitted with the Voigt functions of the same Lorentzian and Gaussian widths. The KL^1 satellite line is fitted with a single Voigt function by setting all parameters free. The background is described by a straight line.

ity, and also for the detector efficiency. These corrections generally depend on the energy difference between the satellite and the diagram line. Since the difference was very small [$\Delta E(KL^1\text{-}K\alpha_1)=25.6$ eV for Ca and 42.3 eV for Fe], these effects were almost negligible (the correction was less than 1%).

IV. METHOD OF DEDUCING THE *L*-SHELL IONIZATION PROBABILITIES

We showed that in the independent-particle framework, the L-shell ionization probability for near-central proton collisions with low-Z atoms can be evaluated from the relative yields of the KL^1 satellite lines [Eq. (4)]. However, the quantities that follow from the measurements reflect the situation in the L shell at the moment of the K x-ray emission. In order to find the ionization probabilities, we have to take into account the rearrangement of inner shell vacancies prior to the K x-ray emission. This process alters the primary vacancy distribution produced in the collision. In the case of low Z-elements where we cannot resolve contributions from the different L subshells, the rearrangement between the subshells is not important. The original vacancy distribution of the L shell is essentially altered by vacancy promotion to higher shells (mainly M). Since the energy shift of the satellite line decreases with the principal quantum number of the spectator vacancy, the energy shifts of the KM^1 satellite lines are much smaller than for the KL^1 satellites. For low-Z elements, the energy shifts of the KM^1 satellite lines are comparable to the $K\alpha$ natural linewidth, so they cannot be resolved from the diagram line. Vacancy promotion into higher shells actually redistributes some of the KL^1 satellite lines into the diagram lines. The second important effect that has to be taken into account concerns the partial fluorescence yield for the $K\alpha$ transition since it may vary due to the presence of additional vacancies in the L shell that is involved in the transition. Considering both effects, the yield of the KL^1 satellite lines relative to the $K\alpha$ diagram line can be expressed as [7]

$$I_1^X=\frac{\sigma_{KL^1}^X}{\sigma_{KL^0}^X}=\frac{\{\sigma_{KL^1}[1-R(L^1)]\}\omega_{K\alpha}(L^n)}{[\sigma_{KL^0}+\sigma_{KL^1}R(L^1)]\omega_{K\alpha}(L^0)}, \tag{5}$$

where I_1^X is the relative yield of the KL^1 satellite line extracted from the fitting procedure and corrected for absorption in the target and on the way to detector, R is the rearrangement factor, and $\omega_{K\alpha}$ is the partial fluorescence yield for the $K\alpha$ transition. The rearrangement factor R is defined as

$$R=\frac{\Gamma_L^A+\Gamma_L^R}{\Gamma_L+\Gamma_K} \tag{6}$$

and the partial fluorescence yield for the $K\alpha$ transition is defined as

$$\omega_{K\alpha}=\frac{\Gamma_{K\alpha}^R}{\Gamma_K}, \tag{7}$$

where Γ_i is the total atomic level width of the particular shell, while Γ_i^R and Γ_i^A are the partial widths for the radiative and Auger transition processes of the shell, respectively. In Eq. (6), the influence of Coster-Kronig transitions is ne-

TABLE I. Ratio of the $K\alpha$ partial fluorescence yields for doubly (KL^1) and singly ionized atoms. The level widths for doubly ionized atoms were calculated according to a statistical procedure [25].

Element	Z	$\omega_{K\alpha}(L^1)/\omega_{K\alpha}(L^0)$
Ca	20	1.010
Ti	22	1.011
Cr	24	1.009
Fe	26	1.013

glected since these transitions redistribute the vacancies between different L subshells, but they do not change the total number of L-shell vacancies produced in the collision. The relative vacancy yield (4) of the KL^1 satellite produced in a near-central proton collision with a low-Z atom can be expressed as

$$\frac{I_{KL^1}}{I_{KL^0}}=\frac{\sigma_{KL^1}}{\sigma_{KL^0}}=\frac{8p_L(0)}{1-p_L(0)} =I_1^X\frac{\omega_{K\alpha}(L^0)}{\left[1-R(L^1)\left(1+I_1^X\frac{\omega_{K\alpha}(L^0)}{\omega_{K\alpha}(L^1)}\right)\right]\omega_{K\alpha}(L^1)}. \quad (8)$$

For the estimation of $\omega_{K\alpha}(L^1)$ and $R(L^1)$ in Eq. (8), it is necessary first to estimate the level width of the KL^1 ionized state. As the level width of the K shell is influenced by an additional L-shell vacancy, the respective tabulated values have to be modified by a suitable correction. We used the statistical method of Larkins [25], where the width of a certain transition is in the first approximation proportional to the number of electrons available for the transition. It has been shown that this approach gives very realistic results for the K-shell level widths [26,27]. For the radiative and nonradiative transition widths in a singly ionized atom we used the values of Scofield [28], Kostroun, Chen, and Crasemann [29], and McGuirre [30,31]. For the $K\alpha$ transition, the fluorescence yields for atoms having an additional vacancy in the L shell (i.e., corresponding to the KL^1 satellite) are shown in Table I. The data are normalized with respect to the KL^0 values and it is apparent that an additional L-shell vacancy does not change the fluorescence yield significantly for low-Z elements. The change in $\omega_{K\alpha}$ can be neglected in the first approximation.

The rearrangement influences the primary vacancy yield to a much higher extent than the variations of the fluorescence yield. We estimated the Z dependence of the rearrangement factor $R(L^1)$ using first the level widths for singly ionized atoms [28–31] and ignored the differences between the L subshells. The result of this estimation, demonstrating the size of the effect only, is shown in Fig. 3. As Fig. 3 suggests, the original vacancy distribution can be changed significantly prior to the K x-ray emission. This strong rearrangement process originates mainly in the competitive LMM Auger transitions, which have level widths comparable to those for the K radiative transition. Though a more realistic calculation of the rearrangement factor using the K-shell level widths of the doubly (KL^1) ionized atom would yield somewhat smaller values, it is apparent that the

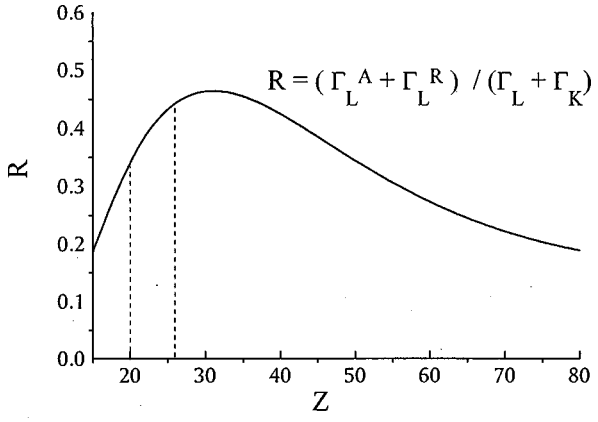

FIG. 3. Z dependence of the rearrangement factor $R=(\Gamma_L^A+\Gamma_L^R)/(\Gamma_K+\Gamma_L)$ calculated from the level widths of singly ionized atoms [23–26].

rearrangement of the L-shell vacancies prior to the K x-ray emission is extremely important. Its influence cannot be neglected, especially for the case of elements of Z around 30.

The rearrangement factor was calculated more precisely for the elements Ca, Ti, Cr, and Fe. The tabulated values for the level widths in singly ionized atoms [28–31] were corrected for the additional hole in the L shell according to the method of Larkins, as explained above. The values are collected in Table II.

In addition to the direct Coulomb ionization, the shake process may also contribute to satellite production. The removal of an inner-shell electron causes a sudden change in the atomic potential that can result in the ejection of an electron to the continuum (shakeoff). The KL^1 satellite yield is therefore composed of direct ionization and shake contributions. Since the L-shell ionization probabilities are rather small for proton impact ($\sim 1\%$ for low-Z elements) and Eq. (4) relates to the L-shell ionization probability independently of its mechanism, we can write the probability obtained from the KL^1 satellite yield as a sum of probabilities

$$p_L=p_L^{\mathrm{DI}}+p_L^S. \quad (9)$$

where DI and S refer to the direct ionization and shake process, respectively. In order to obtain the direct ionization probabilities, we subtracted the shake probabilities from our experimental values. We used the probabilities of Mukoyama and Taniguchi [32] that were calculated using the Hartree-Fock-Slater wave functions within the sudden approximation model. The shake probabilities extend from

TABLE II. Rearrangement factor $R=(\Gamma_L^A+\Gamma_L^R)/(\Gamma_K+\Gamma_L)$ in Ca, Ti, Cr, and Fe for doubly (KL^1) ionized atoms. The level widths for doubly ionized atoms were calculated according to a statistical procedure [25].

Element	Z	R
Ca	20	0.260
Ti	22	0.271
Cr	24	0.281
Fe	26	0.331

TABLE III. L-shell ionization probabilities for the direct Coulomb ionization of Ca, Ti, Cr, and Fe induced in near-central proton collisions

E_p (MeV)	$p_{L(\mathrm{Ca})}(0)$ (%)	$p_{L(\mathrm{Ti})}(0)$ (%)	$p_{L(\mathrm{Cr})}(0)$ (%)	$p_{L(\mathrm{Fe})}(0)$ (%)
0.7	1.30±0.18	0.88±0.13		
0.8	1.27±0.18	0.92±0.14	0.66±0.11	0.43±0.09
0.9	1.29±0.18	0.95±0.14	0.68±0.11	0.47±0.10
1.0	1.31±0.18	0.95±0.14	0.73±0.12	0.53±0.11
1.1	1.27±0.18	0.96±0.14	0.75±0.12	0.56±0.12
1.2	1.27±0.18	0.99±0.15	0.79±0.13	0.60±0.12
1.3	1.27±0.18	0.96±0.14	0.81±0.13	0.64±0.13
1.4	1.25±0.18	0.99±0.15	0.82±0.13	0.66±0.14
1.5	1.23±0.17	1.01±0.15	0.83±0.13	0.69±0.14
2.0		0.86±0.26		
3.0		0.70±0.11		
4.0		0.51±0.08		

0.09% for Fe up to 0.18% for Ca and represent about 13–20% of the direct ionization probability values.

V. RESULTS AND DISCUSSION

Following the procedure outlined above, the L-shell ionization probabilities for the direct Coulomb ionization in central collisions were evaluated from the measured KL^1 satellite yields. As mentioned previously, the elements of interest were Ca, Cr, and Fe ionized with (0.7–1.5)-MeV protons and Ti ionized with (0.7–4)-MeV protons. The ionization probabilities are collected in Table III. The uncertainties of the deduced probabilities are mainly the result of the uncertainties of the level widths used for calculation of the rearrangement factors. In particular, the level widths for LMM and some KLL Auger transitions have large uncertainties, which yield a total uncertainty of the rearrangement factor up to 40%. The uncertainty contribution originating from the fitting procedure is generally less important.

The L-shell ionization probabilities are plotted in Fig. 4 as a function of proton energy in the range 0.7–1.5 MeV. In this energy region the projectile velocity surpasses the L-shell electron velocity ($\eta = 0.76-1.49$). Figure 4 indicates that the ionization probability increases with proton energy in Fe and Cr, reaches a maximum in Ti, and starts to decline in Ca. As expected, the ionization probability reaches a maximum around matching of the projectile and electron velocities. According to Fig. 4, this maximum occurred at slightly larger projectile velocities in our experiment.

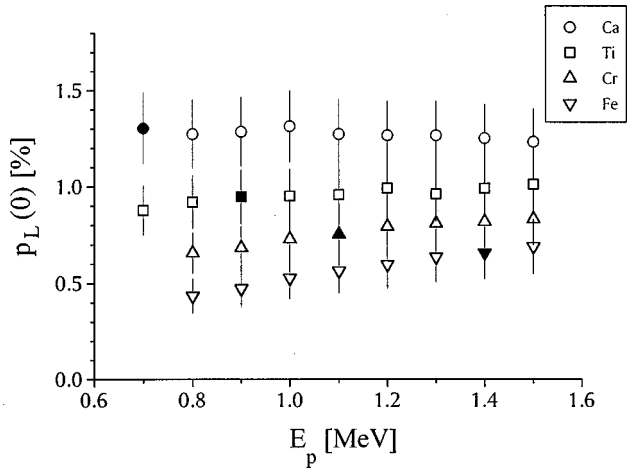

FIG. 4. L-shell ionization probabilities for the direct Coulomb ionization of Ca, Ti, Cr, and Fe induced in near-central collisions with (0.7–1.5)-MeV protons. The impact energies correspond to reduced projectile velocities η in the range 0.76–1.49. The points that correspond to the reduced projectile velocity matching the L-shell electron velocity ($\eta = 1$) are plotted with solid symbols.

For proton-induced ionization of low-Z elements, the predominant ionization mechanism is direct Coulomb ionization. As we are interested in the ionization probability at zero impact parameter, the respective theoretical values have to be obtained in the semiclassical approximation, which allows us to calculate the impact-parameter dependence of the single-electron ionization probability.

The experimental values were compared to the first-order SCA calculations of Trautmann and Rösel [11,12], Šmit [13,14], and Halabuka, Perger, and Trautmann [15]. All these calculations employ classic hyperbolic trajectories, but differ in the choice of atomic wave functions. The codes of Trautmann and Rösel and that of Šmit employ screened hydrogenic Dirac wave functions, but use different approximations for the screening of outer atomic electrons. The wave functions of Šmit are essentially those used traditionally in the plane-wave methods [22,33] and include transitions into the final states with negative energy. As pointed out by Kocbach [34], these states are a good approximation for single-particle states in the self-consistent field. In the calculation of Halabuka, Perger, and Trautmann [15], the concise relativistic Hartree-Fock wave functions were employed.

The theoretical values of the L-shell ionization probability were calculated for the near-zero impact-parameter values (100–150 fm) in order to avoid a large recoil contribution in exactly central collisions. The energy dependence of the experimental and theoretical values for a Ti target is shown in Fig. 5 and the reduced velocity dependence of the ratios between the experimental and theoretical values is given in Fig. 6.

The probabilities calculated by the three methods have a similar energy dependence, though they differ significantly in size. The values of Trautmann and Rösel [11,12] are gen-

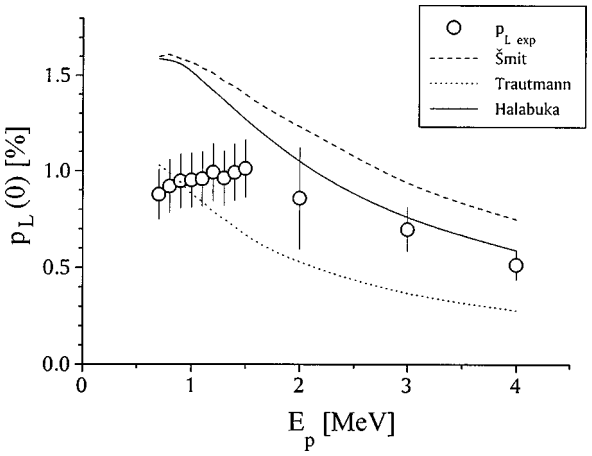

FIG. 5. L-shell ionization probabilities for the direct Coulomb ionization of Ti as a function of the proton energy. The experimental data are compared with the SCA calculations of Trautmann and Rösel [11,12] (dotted line), Šmit [13,14] (dashed line), and Halabuka, Perger, and Trautmann [15] (solid line).

erally a factor of 1.5–2 lower than the values of Šmit [13,14] and Halabuka, Perger, and Trautmann [15]. The latter two differ by a few percent at low collision velocities and by 30% at high collision velocities. However, the differences at high velocities may be up to 10% higher since the calculation [13,14] involved multipoles up to $l=2$ only.

In comparison with the Ti experimental data (Fig. 5), the values of Trautmann and Rösel cross the experimental data at $E_p=1$ MeV ($\eta\sim1$), as their trend is continuously decreasing. The experimental data show a broad maximum at $E_p=1.5$ MeV. A maximum, though of larger intensity and at lower energies, is indicated by the methods of [13,14] and [15]. For higher energies, $E_p>2$ MeV, the experimental data are rather well reproduced by the values of [15], the difference between the two sets of data being smaller than the experimental uncertainties.

The results of Figs. 5 and 6 suggest that the calculation [15] employing relativistic Hartree-Fock wave functions yields data that are closest to experiment. For the method of [13,14], which uses a simple yet effective approximation for the states in the atomic potential, the differences between theory and experiment are 30% larger. This indicates that the proper choice of wave functions is essential for the calculation of ionization probabilities at near-zero impact parameters.

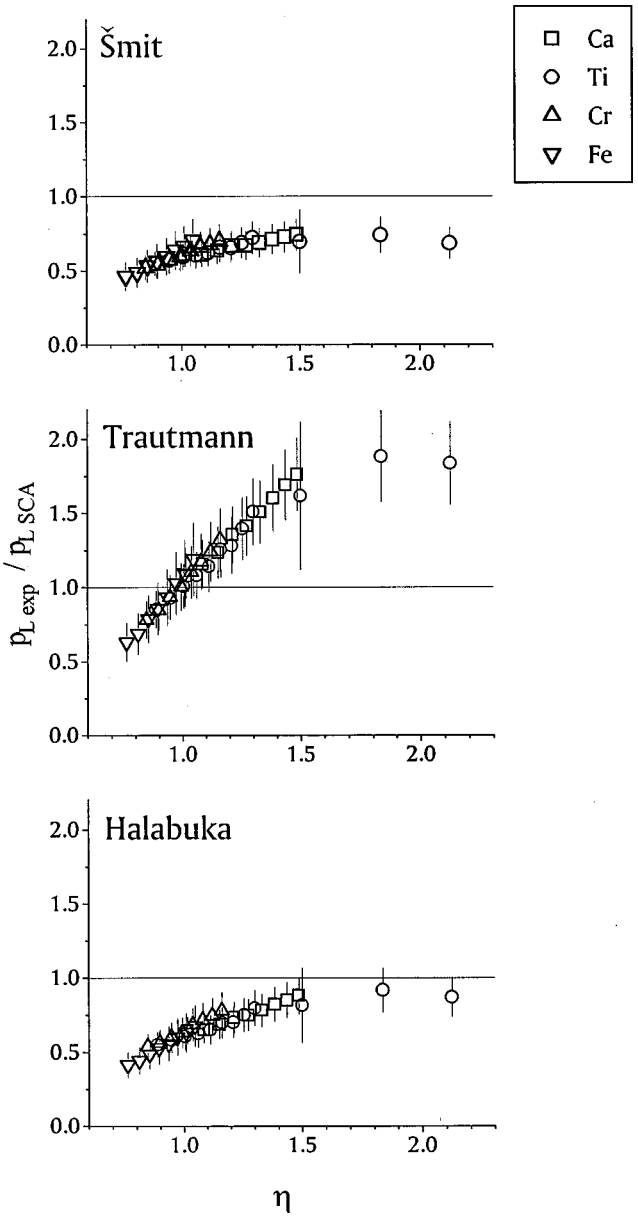

FIG. 6. Ratio of the experimental and theoretical SCA ionization probabilities as a function of the reduced projectile velocity. The three models differ in the choice of wave functions used and employ in turn two different types of hydrogenic Dirac wave functions (see [11,12] and [13,14], respectively) and relativistic Hartree-Fock wave functions [15].

VI. SUMMARY AND CONCLUSIONS

High-resolution measurements of the $K\alpha$ line shape were performed for Ca, Ti, Cr, and Fe targets bombarded by protons. The proton energies were 0.7–1.5 and 0.7–4.0 MeV for the Ti target. The relative KL satellite yields were used to determine the L-shell ionization probabilities in near-central collisions. The method represents a more severe test of the theoretical models than measurements of the total cross sections.

The importance of the rearrangement process due to the L Auger transitions has been demonstrated for low-Z elements ($R=0.26$ for Ca and 0.33 for Fe). It has been shown that the change in the K-shell fluorescence yield due to the additional L-shell spectator vacancy can be neglected. The direct Coulomb ionization probabilities were determined from the satellite yields after subtracting the shake contribution. For proton-induced ionization of low-Z elements, the shake probabilities are comparable to the direct L-shell ionization probabilities.

The experimental results obtained were compared with the SCA calculations. The calculated values depend strongly on the wave functions used. The comparison supports the use of relativistic Hartree-Fock wave functions. In the low-energy region ($\eta<1.5$), the current SCA calculations fail to

reproduce the measured values, regardless of the type of wave function used.

ACKNOWLEDGMENTS

The authors acknowledge the kindness of the staff of the Nuclear Microanalysis Laboratory of R. Bošković Institute, Zagreb, in offering the Tandem accelerator facility for measurements of Ti data in the (2–4)-MeV energy region. M.K. wishes to express particular thanks for kind hospitality during his visit to the Basel University group. He would also like to thank A. Mühleisen and B. Zorko for a critical reading of the manuscript. The work was mainly supported by the Slovenian Ministry of Science and Technology (Project No. J1-7473).

[1] R. L. Watson, F. E. Jenson, and T. Chiao, Phys. Rev. A **10**, 1230 (1974).
[2] R. L. Watson, B. I. Sonobe, J. A. Demarest, and A. Langenberg, Phys. Rev. A **19**, 1529 (1979).
[3] K. W. Hill, B. I. Doyle, S. M. Shafroth, D. H. Madison, and R. D. Deslattes, Phys. Rev. A **13**, 1334 (1976).
[4] C. F. Moore, M. Senglaub, B. Johnson, and P. Richard, Phys. Lett. **40A**, 107 (1972).
[5] R. L. Kaufmann, J. H. McGuire, and P. Richard, Phys. Rev. A **8**, 1233 (1973).
[6] N. Cue, V. Dutkiewicz, P. Sen, and H. Bakhru, Phys. Lett. **46A**, 159 (1973).
[7] P. Rymuza, Z. Sujkowski, M. Carlen, J.-Cl. Dousse, M. Gasser, J. Kern, B. Perny, and Ch. Rhéme, Z. Phys. D **14**, 37 (1989).
[8] P. Rymuza, T. Ludziejewski, Z. Sujkowski, M. Carlen, J.-Cl. Dousse, M. Gasser, J. Kern, and Ch. Rhéme, Z. Phys. D **23**, 81 (1992).
[9] D. F. Anagnostpoulos, J. Phys. B **25**, 2771 (1992).
[10] M. W. Carlen, M. Polasik, B. Boshung, J.-Cl. Dousse, M. Gasser, Z. Halabuka, J. Hoszowska, J. Kern, B. Perny, Ch. Rhéme, P. Rymuza, and Z. Sujkowski, Phys. Rev. A **46**, 3893 (1992).
[11] D. Trautmann and F. Rösel, Nucl. Instrum. Methods **169**, 259 (1980).
[12] D. Trautmann and F. Rösel, Nucl. Instrum. Methods Phys. Res. **214**, 21 (1983).
[13] Ž. Šmit and I. Orlić, Phys. Rev. A **50**, 1301 (1994).
[14] Ž. Šmit Phys. Rev. A **53**, 4145 (1996).
[15] Z. Halabuka, W. Perger, and D. Trautmann, Z. Phys. D **29**, 151 (1994).
[16] V. Cindro, M. Budnar, M. Kregar, V. Ramšak, and Ž. Šmit, J. Phys. B **22**, 2161 (1989).
[17] M. Budnar, A. Mühleisen, M. Hribar, H. Janžekovič, M. Ravnikar, Ž. Šmit, and M. Žitnik, Nucl. Instrum. Methods Phys. Res. B **63**, 377 (1992).
[18] M. Budnar and A. Mühleisen, Nucl. Instrum. Methods Phys. Res. B **75**, 81 (1993).
[19] P. Richard, in *Atomic Inner Shell Processes*, edited by B. Crasemann (Academic, New York, 1975), p. 104.
[20] Y. Cauchois and C. Senemaud, *Wavelengths of X-Ray Emission Lines and Absorption Edges* (Pergamon, Oxford, 1978).
[21] J. Végh, EWA, A spectrum evaluation program for XPS and UPS, in *Proceedings of the Sixth European Conference on Applications of Surface and Interface Analysis, Montreaux, 1995*, edited by H. J. Mathieu, B. Reihl, and D. Briggs (Wiley, Chicester, 1996), pp. 679–682.
[22] E. Merzbacher and H. W. Lewis, in *Encyclopedia of Physics*, edited by S. Flugge, Handbuch der Physik Vol. 34 (Springer, Berlin, 1958), p. 166.
[23] J. F. Ziegler and J. Manoyan, Nucl. Instrum. Methods Phys. Res. B **35**, 215 (1988).
[24] T. P. Thinh and J. Leroux, X-Ray Spectrom. **8**, 85 (1979).
[25] F. P. Larkins, J. Phys. B **4**, L29 (1971).
[26] D. F. Anagnostopoulos, Ph.D. thesis, Forschung Zentrum Jülich, 1992 (unpublished).
[27] D. F. Anagnostopoulos, J. Phys. B **28**, 47 (1995).
[28] J. H. Scofield, Phys. Rev. **179**, 9 (1969).
[29] V. O. Kostroun, M. H. Chen, and B. Crasemann, Phys. Rev. A **3**, 533 (1969).
[30] E. J. McGuirre, Phys. Rev. A **3**, 587 (1971).
[31] E. J. McGuirre, Phys. Rev. A **3**, 1801 (1971).
[32] T. Mukoyama and K. Taniguchi, Phys. Rev. A **36**, 693 (1987).
[33] D. Jamnik and Č. Zupančič, K. Dan. Vidensk. Selsk. Mat. Fys. Medd. **31**, 2 (1957).
[34] L. Kocbach, J. M. Hansteen, and R. Gundersen, Nucl. Instrum. Methods **169**, 281 (1980).